Influence of grain size on the flow properties of an Al-Mg-Sc alloy over seven orders of magnitude of strain rate

Pedro Henrique R. Pereira, Ying Chun Wang, Yi Huang, Terence G. Langdon

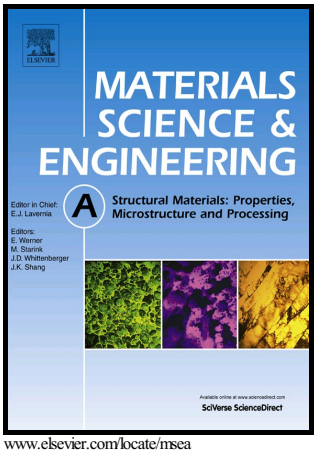

www.elsevier.com/locate/msea

PII: S0921-5093(17)30021-7
DOI: http://dx.doi.org/10.1016/j.msea.2017.01.020
Reference: MSA34582

To appear in: *Materials Science & Engineering A*

Received date: 10 November 2016
Revised date: 5 January 2017
Accepted date: 6 January 2017

Cite this article as: Pedro Henrique R. Pereira, Ying Chun Wang, Yi Huang and Terence G. Langdon, Influence of grain size on the flow properties of an Al-Mg Sc alloy over seven orders of magnitude of strain rate, *Materials Science & Engineering A,* http://dx.doi.org/10.1016/j.msea.2017.01.020

Influence of grain size on the flow properties of an Al-Mg-Sc alloy over seven orders of magnitude of strain rate

Pedro Henrique R. Pereira[a,b], Ying Chun Wang[c], Yi Huang[a*], Terence G. Langdon[a]

[a]Materials Research Group, Faculty of Engineering and the Environment, University of Southampton, Southampton SO17 1BJ, U.K.
[b]CAPES Foundation, Ministry of Education of Brazil, Brasília - DF 70040-020, Brazil.
[c]School of Materials Science and Engineering,
Beijing Institute of Technology, Beijing 100081, China.
[*]Corresponding author: Yi Huang email: y.huang@soton.ac.uk

Abstract

Experiments were conducted to evaluate the flow properties of an Al-3Mg-0.2Sc alloy both without and with processing using equal-channel angular pressing (ECAP). The initial grain size was ~300 μm and this was reduced to ~250 nm by ECAP and then increased to ~600 nm by annealing at 673 K for 10 min. Tests were conducted to determine the mechanical properties over seven orders of magnitude of strain rate from ~10^{-4} to ~10^{3} s^{-1}. The results confirm the validity of the Hall-Petch relationship in the material processed by ECAP. Shear banding occurred in the coarse-grained material during dynamic testing but in the ECAP-processed alloy there was only minor grain coarsening. There was evidence for dynamic strain ageing in both the coarse and the ultrafine-grained (UFG) alloy with a transition in flow mechanism at high temperatures from dislocation climb in the coarse-grained material to superplasticity in the UFG alloy.

Keywords: aluminium alloys; dynamic testing; equal-channel angular pressing; Hall-Petch relationship; superplasticity.

1. Introduction

The increasing demand for more fuel-efficient and environmentally-friendly vehicles has motivated the development of light-weight aluminium alloys especially designed for applications in the transportation industry [1]. Processing by severe plastic deformation (SPD) [2,3], as in equal-channel angular pressing (ECAP) [4] and high-pressure torsion (HPT) [5] has been successfully used to produce ultrafine-grained (UFG) Al alloys with remarkably improved properties by comparison with metals subjected to conventional metal forming [6].

Pure aluminium processed by ECAP displays superior mechanical strength and higher strain rate sensitivity compared with the coarse-grained material [7]. Similar enhancements are also observed in SPD-processed Al-Mg alloys [8-20] which exhibit additional strengthening and grain refinement due to the presence of Mg solutes. However, Al-Mg alloys have unstable grain structures at high temperatures after SPD processing and any benefits in the mechanical properties attained by grain refinement are lost through early recrystallization [7,21-24]. With the aim of improving the grain boundary stability of Al alloys processed by SPD, the materials may be alloyed with Sc additions because Al_3Sc dispersoids are effective in pinning the grain boundaries and retaining a UFG structure even at elevated temperatures [24-29].

The Al-Mg-Sc alloys have attracted significant attention because of their high strength to density ratio as well as their excellent superplastic properties [30,31]. Although the superplastic properties of Al-Mg-Sc alloys were studied extensively after ECAP [24,25,28,32-37] and HPT [38-41], there are only limited studies documenting the mechanical properties of UFG Al-Mg-Sc alloys at ambient temperatures [42-45].

Recent studies have demonstrated the outstanding capacity of Al alloys with Sc additions to resist the impact of high speed projectiles [46,47] which makes this material a major candidate for use in the structure of spacecraft. Although several investigations were reported evaluating the mechanical behaviour at dynamic strain rates in several UFG metals

[48-58], there are no reports are at present available on the deformation of SPD-processed Al-Mg-Sc alloys at high strain rates. Accordingly, this investigation was initiated to assess the mechanical properties and deformation mechanisms in Al-Mg-Sc alloys tested under quasi-static and dynamic conditions. The validity of the Hall-Petch relationship and the influence of grain size on the mechanical behaviour were also examined.

2. Experimental material and procedures

2.1 Material and processing

An Al-3% Mg-0.2% Sc (in wt. %) alloy was supplied by China Rare Metal Material Corporation (Jiangxi Province, China) in the form of forged bars having lengths of 130 mm and diameters of 10 mm. These bars were solution treated at 880 ± 2 K for 1 h and then quenched in water. Billets with lengths of ~65 mm were cut from the bars, lubricated with MoS_2 and then processed by ECAP for 8 passes using route B_c in which each billet is rotated by 90° in the same sense between passes [59]. The processing was conducted at room temperature using a pressing speed of ~2 mm s^{-1} and a solid die having an internal channel angle of 90º and an outer arc of curvature of ~20º. These angles introduce a strain of ~1 on each pass [60].

2. Mechanical testing

For mechanical testing, samples were machined from both the solution treated and the ECAP-processed billets as depicted in Fig. 1 where the *X*, *Y*, *Z* coordinate system is defined in Fig. 1(a). Discs with thicknesses of ~1.0 mm were cut from these billets and ground using abrasive papers to thicknesses of ~0.8 mm. Thereafter, two tensile specimens were machined from each disc using electrical discharge machining and these specimens were pulled to failure using a Zwick Z030 testing machine operating at a constant rate of cross-head displacement. Tests were conducted at temperatures of 298, 523 and 673 K using initial strain rates, $\dot{\varepsilon}$, from 3.3×10^{-4} to 1.0×10^{-1} s^{-1}. All samples were held at the testing temperature for

~10 min prior to application of the load and the temperatures were held constant to within ±2 K during testing.

Cylindrical samples with lengths of 5 mm and diameters of 5 mm were machined from both the solution treated and the ECAP-processed metal such that their longitudinal axes lay along the pressing direction. These specimens were tested dynamically at temperatures from 298 to 673 K using a strain rate of 4.0×10^3 s^{-1} in a split Hopkinson pressure bar (SHPB) facility using the procedure described earlier [53]. Prior to dynamic testing, the samples were heated and held at the required temperature for ~10 min. All dynamic testing was performed on at least two different specimens under the same experimental conditions to ensure the reproducibility of the data.

The stress, σ, and strain, ε, were initially calculated during dynamic testing based on the incident, reflected and transmitted strain pulses using the relationships presented in other reports [53,61]. Thereafter, as dynamic testing using the SHPB is adiabatic, the temperature rise, ΔT, during plastic straining was calculated from [62]

$$\Delta T(t) = \frac{0.9}{\rho_s c_s} \int_0^{\varepsilon(t)} \sigma(t)\, d\varepsilon \quad (1)$$

where ρ_s and c_s are the density and the specific heat capacity of the sample, respectively. For this investigation, ΔT was estimated using Eq. (1) with $\rho_s = 2.7 \times 10^3$ kg m^{-3} and $c_s = 9 \times 10^3$ J kg^{-1} K^{-1} [63] and the isothermal true stress, σ_{iso}, henceforth denoted the true stress, was estimated using [51]

$$\sigma_{iso}(t) = \sigma(t) - \frac{\partial \sigma}{\partial T} \Delta T(t) \quad (2)$$

2.3 Microstructural characterization

The microstructure of the Al-Mg-Sc alloy was examined by scanning electron microscopy (SEM) and electron backscattered diffraction (EBSD). Samples were ground, polished using 1 μm diamond paste and 0.06 μm silica colloidal and then etched using an aqueous solution of 5% HBF_4.

The grain structure of the Al-Mg-Sc alloy immediately after ECAP processing was observed using a JSM6500F thermal field emission SEM and the average grain size was estimated from the grain boundary spacing, $\bar{L}$, determined using the linear intercept method. EBSD patterns were collected using step sizes smaller than 4 and 0.2 μm for the solution treated and ECAP-processed materials, respectively. A cleaning procedure, including grain dilatation and grain confidence index standardization, was performed on each OIM image such that the total number of modified points was <20 % for all points measured. Low-angle grain boundaries (LAGBs) were defined as having misorientation differences between adjacent points from 2º to 15° and high-angle grain boundaries (HAGBs) had misorientations >15°. The OIM analysis generated graphical displays of texture using pole figures from each measurement area. In addition, the distributions of the correlated misorientation angles were calculated for each condition.

3. Experimental results

3.1 Mechanical properties

Representative plots of true stress vs true strain are shown in Fig. 2 for samples with and without processing by ECAP when testing dynamically using the SHPB system. The curves show that processing by ECAP leads to superior mechanical strength at all testing temperatures. In addition, the curves of the solution treated material display significant work-hardening at 298 K whereas the curves at 523 and 673 K exhibit only minor work-hardening and achieve similar true stresses of ~200 MPa at $\varepsilon = 0.3$. There is an apparent saturation in the true stress at ~520 MPa for the ECAP-processed alloy tested at 298 K and there are only minor decreases in the flow stresses for $T \leq 573$ K.

In order provide information on the deformation mechanisms, Fig. 3 shows the variation with strain rate of the true stress at $\varepsilon = 0.05$ for samples tested at different absolute temperatures, *T*, in (a) the solution treated condition and (b) after ECAP processing. The

slopes of these curves correspond to the strain rate sensitivity, m (= $[\partial \log \sigma / \partial \log \dot{\varepsilon}]_T$), and it is apparent that there is a negative strain rate sensitivity of $m \approx -0.04$ for the unprocessed alloy tested at 298 K for strain rates below ~3.3×10^{-1} s^{-1}. This negative value of m is associated with the occurrence of dynamic strain ageing (DSA) in the Portevin-Le Chatelier effect [18,19,64-66]. Inspection of Fig. 3(a) shows that $m > 0$ in the solution treated alloy from 3.3×10^{-4} to 3.3×10^{-1} s^{-1} at 523 and 673 K, the slopes of the curves increase with increasing T and decreasing $\dot{\varepsilon}$, and the value of m is ~0.2 at strain rates below ~3.3×10^{-2} s^{-1}.

In Fig. 3(b) for the ECAP-processed material there is an approximate sigmoidal relationship at the two higher temperatures which is similar to the three regions of flow generally observed in superplastic metals [67]. At the lowest strain rates at $\dot{\varepsilon} \leq 1.0 \times 10^{-3}$ s^{-1} the curves have a slope of ~0.2 whereas at faster strain rates, up to $\dot{\varepsilon} \approx 3.3 \times 10^{-1}$ s^{-1} for the specimens tested at 523 K, the slope is $m \approx 0.5$. At even faster strain rates, the values of m remain positive but tend to decrease with increasing strain rate.

3.2 Grain structure and texture of the coarse-grained Al-Mg-Sc alloy

Typical OIM images are shown in Fig. 4 obtained along the X plane in the middle-section of (a) the unprocessed alloy and after dynamic testing at (b) 298 and (c) 673 K. Inspection of Fig. 4(a) shows that the solution treated material has a fairly homogeneous microstructure with $\bar{L} \approx 300$ μm. In Figs 4(b) and (c), there is evidence for the development of substructure with LAGBs in the highly strained areas and there are strong texture gradients which reflect abrupt changes in the local misorientations. These structures initially form LAGBs but eventually evolve into grains with HAGBs through mechanically-induced dynamic recrystallization (DRX) [48,49,68]. It also follows from Fig. 4 (b) that some grains essentially preserve their original sizes and have a very high density of LAGBs. There is a distinct texture in these grains with the {110} planes parallel to the X plane. Similarly, Fig.

4(c) shows many large grains with the same texture as in Fig. 4(b) but with a lower density of LAGBs.

The textures of the unprocessed alloy are presented as {111} pole figures in Fig. 5 both (a) without and (b,c) with dynamic testing. Thus, the alloy has a random texture after solution treatment but it develops a deformation texture after dynamic testing at (b) 298 and (c) 673 K. This texture is typical of fcc metals with high stacking fault energies after compression testing and it is characterized by a fibre-type texture where the compression axis is the fibre axis [69,70]. As is evident from Figs. 5(b) and (c), both samples show a strong texture component around {110} and, for the alloy tested at 298 K, there is also a weak texture component around {100}.

3.3 Grain structure and texture of the UFG Al-Mg-Sc alloy

The microstructure of the alloy was intensively refined by 8 ECAP passes to give $\bar{L} \approx$ 250 nm as measured by SEM where this is comparable to the grain size of ~200 nm reported earlier for the same alloy using transmission electron microscopy after processing through similar conditions [33]. Figure 6 shows OIM images of the ECAP-processed alloy (a) after annealing at 673 K for 10 min, (b) after tensile testing at 3.3×10^{-3} s^{-1} at 673 K and (c and d) after dynamic testing at 4.0×10^{3} s^{-1} at 298 and 673 K, respectively. It follows from Fig. 6(a) that the banded structures formed during ECAP evolve into nearly equiaxed grains during annealing at 673 K and, in addition, there is a large fraction of subgrains with an average size of ~0.6 μm.

In Fig. 6 (b) the UFG alloy pulled to failure at 3.3×10^{-3} s^{-1} at 673 K shows mostly grains with HAGBs. In addition, EBSD scanning was performed in the gauge area of a tensile specimen which underwent an elongation of ~980 %. As elongations >400 % were observed in this condition [71], the randomness of the texture and the high misorientations between neighbouring grains suggests that the ECAP-processed alloy deforms by grain boundary

sliding (GBS) at this temperature and strain rate. It also follows from Figs. 6(c) and (d) that a strong texture component develops around {110} after dynamic testing regardless of the testing temperature. It is also apparent that the grains are equiaxed and primarily consist of HAGBs although there is a significant fraction of LAGBs.

The fractions of boundaries are plotted in Fig. 7 as a function of the misorientation angles for the samples tested under the same conditions as in Fig. 6: these histograms depict the correlated pixel-to-pixel misorientation distributions with a cut-off angle of 2° [72] and the superimposed solid curves represent the Mackenzie theoretical distribution [73]. It is apparent from Fig. 7(a) that the alloy has a high fraction of LAGBs (~30 %) after ECAP and annealing at 673 K. Similarly, after dynamic testing there are also large fractions of LAGBs as shown in Figs 7(c) and (d) and the material also has a larger fraction of HAGBs with misorientation angles >50° compared with the annealed material. It is readily seen in Fig. 7(b) that testing in tension at 673 K with a strain rate of 3.3×10^{-3} s^{-1} gives results that conform closely with the Mackenzie distribution [73] thereby demonstrating that the alloy develops a random texture during tensile straining. By contrast, there are very significant deviations from the theoretical curves after dynamic testing in Figs 7(c) and (d) so that a strong texture develops under these conditions as shown by the corresponding {111} pole figures for the four different testing conditions displayed in Fig. 8.

In Fig. 8(a) there is a typical ECAP shear texture [74-77] after ECAP and annealing. Conversely, the pole figure after tensile testing in Fig. 8(b) exhibits a relatively small intensity index as well as a random distribution and this is similar to the same alloy when testing through 8 passes of ECAP using a die with a channel angle of 60° [78]. By contrast, Figs. 8(c) and (d) reveal a strong compression texture with the same characteristics described in Figs. 5(b) and (c) after dynamic testing. Accordingly, as already noted for the OIM images in Figs

6(c) and (d), the {110} planes are mostly parallel to the *X* plane which is normal to the compression axis.

4. Discussion

4.1 Examining the validity of the Hall-Petch relationship in Al-Mg-Sc alloys

The plots depicted in Figs 2 and 3 confirm the superior mechanical strength of the UFG Al-Mg-Sc alloy during deformation at ambient temperature regardless of the testing strain rate. It is well established that the ECAP-processed alloy displays excellent superplastic properties at elevated temperatures [33] and also a significantly higher strength when tested using the SPHB facility by comparison with the coarse-grained material or with a UFG Al-1.5% Mg alloy [51]. The reasons for these exceptional mechanical properties are associated both with the strengthening effects of the Al-Mg solid solution and the presence of many grain boundaries due to the SPD processing and with the presence of Al_3Sc precipitates which enhance the strength and the grain boundary stability of this aluminium-based alloy [31,79]. In addition, it is important to note that Al-Mg alloys without Sc or similar additions exhibit substantial grain growth at temperatures above 500 K [21,22,80] and this is deleterious for the material strength and ductility at high temperatures.

There are numerous reports discussing the validity of the Hall-Petch relationship for materials with grain sizes in the submicrometre range [81-85]. In order to verify whether the grain boundary strengthening predicted by the Hall-Petch relationship remains consistent for the UFG Al-3Mg-0.2Sc alloy, Fig. 9 plots the yield stress, σ_y, against the inverse square root of the grain size using both the experimental data obtained in this investigation and data from other studies conducted on commercially pure aluminium [86-89], Al-Mg alloys [10,18,20,51,90-92] and Al-Mg-Sc alloys [37,42-44,93].

It is apparent from Fig. 9 that pure aluminium (Al 1100) has inferior strength compared with Al-Mg alloys regardless of the grain size. There is also a breakdown in the Hall-Petch relationship at $\bar{L}^{-0.5} \approx 1600$ m$^{-0.5}$ which corresponds to $\bar{L} \approx 0.4$ μm for Al 1100. In

addition, Al-Mg alloys display a delayed breakdown in the Hall-Petch relationship which occurs for grain sizes <0.15 μm. By contrast, the evidence in Fig. 9 infers that the Hall-Petch relationship remains accurate for Al-Mg-Sc alloys over the full range of grain sizes evaluated in this and other studies. This is consistent with earlier results on an Al-5Mg alloy processed by HPT for 10 turns to give a grain size of ~70 nm [94].

The absence of a breakdown in the Hall-Petch relationship suggests that the deformation is primarily controlled by intragranular dislocation motion and the contribution from the emission and annihilation of extrinsic dislocations at the non-equilibrium grain boundaries may be diminished by the presence of Mg segregation at HAGBs and triple junctions [42]. Thus, high concentrations of Mg solutes were detected at grain boundaries in SPD-processed Al-Mg alloys [95-98]. There was also some evidence from SEM in the present study for a thin discontinuous layer of Mg segregates along the grain boundaries in the ECAP-processed Al-Mg-Sc alloy after dynamic testing but a more comprehensive study is now needed to fully substantiate this effect. Nevertheless, as verified through molecular dynamic simulations [99-101], the local atomic structure along HAGBs has a major influence on the stress required for the emission of dislocations and in practice the segregation of Mg along the boundaries serves to reduce the boundary energy and improve the grain stability [102,103]. High concentration of Mg at grain boundaries may also suppress the emission of extrinsic dislocations through solute drag [42].

It is apparent from Fig. 9 that Al-Mg-Sc alloys have superior mechanical strength by comparison with other Al-Mg alloys having similar Mg contents. This is due to the presence of the Al_3Sc dispersoids which act as obstacles for dislocation glide [31]. The experimental data in Fig. 9 was obtained from Al-Mg-Sc alloys processed using different procedures, testing temperatures and strain rates and the experimental points represented by the open

squares are for the ECAP-processed alloy tested at 4.0×10^3 s^{-1}. This confirms that intragranular dislocation slip remains active even at extremely high strain rates.

4.2 The deformation mechanisms in the coarse and UFG Al-Mg-Sc alloys

Al-Mg-Sc alloys deform through different mechanisms depending on grain size, temperature and strain rate. In general, polycrystalline metals develop adiabatic shear bands during deformation at dynamic strain rates [49,53,55,68] and strain localization within these shear bands promotes a mechanically-driven grain refinement [48,49]. In this study, strain localization and local grain refinement were observed in the coarse-grained material after dynamic testing. Therefore, the prominent work hardening of the unprocessed alloy during dynamic deformation at 298 K is attributed to an increase in the dislocation density and the formation of small grains which act as effective barriers to dislocation motion.

Figure 3 shows that the coarse-grained alloy exhibits a negative strain rate sensitivity ($m \approx -0.04$) when testing at 298 K at strain rates lower than $\sim 3.3 \times 10^{-1}$ s^{-1}. Similarly, coarse-grained Al-Mg alloys with different magnesium contents also display $m < 0$ which is due to the occurrence of DSA wherein the flow stress is controlled by interactions between mobile dislocations and solute atom atmospheres [64-66,104-106]. The presence of solutes requires an increment of the local shear stress to promote the movement of dislocations with their solute atmospheres and hence, after application of additional stresses, these dislocations are released and then require lower stresses to continue their movement leading to flow instability. This instability has been demonstrated both in experiments [18,64,66,107] and in computational modelling [108].

It is readily apparent from Fig. 3 that m increases with increasing temperatures and is ~0.2 at a strain rate of $\sim 10^{-3}$ s^{-1}. This value of m is consistent with deformation controlled by dislocation climb at 673 K for strain rates from 3.3×10^{-4} to $\sim 10^{-2}$ s^{-1} and this is in good agreement with data reported for a coarse-grained Al-Mg alloy in mechanical testing [109].

Inspection of Fig 3(b) shows also that $m \approx 0$ for the ECAP-processed alloy metal at 298 K which suggests the occurrence of DSA. In practice, serrated flow and profuse micro-shear bands were observed in Al-Mg-Si [11] and Al-Mg-Mn-Sc [44,45] alloys processed by ECAP and mechanically tested under conditions similar to those in the present investigation and there was also evidence in this work for limited serrated flow at low temperatures and strain rates for the ECAP-processed Al-3Mg-0.2Sc alloy.

During deformation at high temperatures through the mechanism of dislocation climb, subgrains form within the grains and it is well established, for both metals [110] and ceramics [111], that the average subgrain size, λ, is dependent upon stress through the relationship

$$\lambda = \zeta\, b \left(\frac{\sigma}{G}\right)^{-1} \qquad (3)$$

where b is the Burgers vector, G is the shear modulus and ζ is a constant having a value of ~20.

Figure 10 shows a plot of grain size against the modulus-compensated stress, σ/G, for different temperatures and strain rates where the value of σ corresponds to the maximum flow stress in ECAP for an Al-1.5Mg alloy [51] and the Al-3Mg-0.2Sc alloy used in this investigation. The two lower broken lines labelled $\overline{L}_{(0,298\ K)}$ and $\overline{L}_{(0,673\ K)}$ refer to the measured grain sizes in the Al-Mg-Sc alloy of ~250 and ~600 nm immediately after ECAP and after ECAP and annealing at 673 K for 10 min, respectively, and the solid line represents the theoretical prediction for λ using Eq. (3) with ζ = 20, b = 2.86×10^{-10} m and G (MPa) = $(3.022 \times 10^4) - 16T$ [112].

It is readily noted from Fig. 10 that $\overline{L} \geq \lambda$ for UFG Al-1.5Mg and the Al-3Mg-0.2Sc alloy subjected to dynamic testing. It is also apparent from the OIM images in Fig. 6, and from the histograms in Fig 7, that the ECAP-processed samples tested at 4.0 x 10^3 s^{-1} have higher fractions of LAGBs by comparison with the annealed Al alloy. In addition, these LAGBs are mostly organized as subgrains and are more pronounced in the

material tested at 673 K. It follows from Fig. 10 that the subgrain sizes after dynamic testing are slightly larger than immediately before testing. Nevertheless, in addition to the strong deformation texture, the DRX grains are equiaxed and homogeneously distributed as shown in Figs 6(c) and (d). Also, the ECAP-processed alloy exhibits excellent strength and only very limited grain coarsening even after extensive straining at very high strain rates. Therefore, as the Al-3Mg-0.2Sc alloy preserves the grain refinement attained during ECAP processing and no cracks are visible in the compressed samples, it is concluded that the UFG Al-3Mg-0.2Sc alloy is a potential candidate for applications demanding light-weight materials with good ductility and high impact resistance.

5. Summary and conclusions

1. An Al-3% Mg-0.2% Sc alloy was processed by ECAP at room temperature to produce a grain size of ~250 nm. This grain size increased to ~600 nm after annealing for 10 min at 673 K. Mechanical testing was conducted at different temperatures over a very wide range of strain rates up to dynamic testing at 4.0×10^{3} s^{-1}.

2. Excellent mechanical properties were achieved after ECAP processing. The results confirm the validity of the Hall-Petch relationship down to grain sizes of ~0.1 μm.

3. Profuse shear banding and grain refinement were observed in the coarse-grained material during dynamic testing. The ECAP-processed alloy exhibited only minor coarsening and a reasonably uniform distribution of grains after testing at 4.0×10^{-3} s^{-1}.

4. Dynamic strain ageing occurred in both the coarse and UFG Al-Mg-Sc alloy when deforming at 298 K for strain rates below ~10^{-1} s^{-1}. The results suggest dislocation climb as the rate-controlling mechanism for the coarse-grained alloy at 673 K and at strain rates from ~10^{-4} to ~10^{-2} s^{-1}. In the ECAP-processed alloy, the strain rate sensitivity was ~0.5 at low strain rates which is consistent with superplastic flow.

Acknowledgements

This work was supported by CAPES in Brazil, the National Natural Science Foundation of China under Grant No. 51671030 and the European Research Council under ERC Grant Agreement No. 267464-SPDMETALS.

References

[1] W.S. Miller, L. Zhuang, J. Bottema, A.J. Wittebrood, P. De Smet, A. Haszler, A. Vieregge, Recent development in aluminium alloys for the automotive industry, Mater Sci. Eng. A 280 (2000) 37-49.

[2] R.Z. Valiev, R.K. Islamgaliev, I.V. Alexandrov, Bulk nanostructured materials from severe plastic deformation, Prog. Mater. Sci. 45 (2000) 103-189.

[3] T.G. Langdon, Twenty-five years of ultrafine-grained materials: Achieving exceptional properties through grain refinement, Acta Mater. 61 (2013) 7035-7059.

[4] R.Z. Valiev, T.G. Langdon, Principles of equal-channel angular pressing as a processing tool for grain refinement, Prog. Mater. Sci. 51 (2006) 881-981.

[5] A.P. Zhilyaev, T.G. Langdon, Using high-pressure torsion for metal processing: Fundamentals and applications, Prog. Mater. Sci. 53 (2008) 893-979.

[6] I. Sabirov, M.Yu. Murashkin, R.Z. Valiev, Nanostructured aluminium alloys produced by severe plastic deformation: New horizons in development, Mater. Sci. Eng. A 560 (2013) 1-24.

[7] J. May, H.W. Höppel, M. Göken, Strain rate sensitivity of ultrafine-grained aluminium processed by severe plastic deformation, Scripta Mater. 53 (2005) 189-194.

[8] E. Romhanji, M. Dudukovska, D. Glišić, The effect of temperature on strain-rate sensitivity in high strength Al-Mg alloy sheet, J. Mater. Process. Tech. 125-126 (2002) 193-198.

[9] J. Gubicza, N. Q. Chinh, Z. Horita, T. G. Langdon, Effect of Mg addition on microstructure and mechanical properties of aluminium, Mater. Sci Eng. A 387-389 (2004) 55-59.

[10] R. Kapoor, J.K. Chakravartty, Deformation behavior of an ultrafine-grained Al–Mg alloy produced by equal-channel angular pressing, Acta Mater. 55 (2007) 5408-5418.

[11] I. Sabirov, M.R. Barnett, Y. Estrin, P.D. Hodgson, The effect of strain rate on the deformation mechanisms and the strain rate sensitivity of an ultra-fine-grained Al alloy, Scripta Mater. 61 (2009) 181-184.

[12] C. Xu, Z. Horita, T.G. Langdon, Microstructural evolution in an aluminum solid solution alloy processed by ECAP, Mater. Sci Eng. A 528 (2011) 6059-6065.

[13] T. Morishige, T. Hirata, T. Uesugi, Y. Takigawa, M. Tsujikawa, K. Higashi, Effect of Mg content on the minimum grain size of Al–Mg alloys obtained by friction stir processing, Scripta Mater. 64 (2011) 355-358.

[14] A. Loucif, R.B. Figueiredo, T. Baudin, F. Brisset, R. Chemam, T.G. Langdon, Ultrafine grains and the Hall–Petch relationship in an Al–Mg–Si alloy processed by high-pressure torsion, Mater. Sci. Eng. A 532 (2012) 139-145.

[15] Y.J. Chen, Y.C. Chai, H.J. Roven, S.S. Gireesh, Y.D. Yu, J. Hjelen, Microstructure and mechanical properties of Al–xMg alloys processed by room temperature ECAP, Mater. Sci. Eng. A 545 (2012) 139-147.

[16] A.C. Magee, L. Ladani, Temperature dependency of mechanical behavior and strain rate sensitivity of an Al–Mg alloy with bimodal grain size, Mater. Sci. Eng. A 582 (2013) 276-183.

[17] K. Edalati, D. Akama, A. Nishio, S. Lee, Y. Yonenaga, J.M. Cubero-Sesin, Z. Horita, Influence of dislocation–solute atom interactions and stacking fault energy on grain size of single-phase alloys after severe plastic deformation using high-pressure torsion, Acta Mater. 69 (2014) 68-77.

[18] O. Andreau, J. Gubicza, N.X. Zhang, Y. Huang, P. Jenei, T.G. Langdon, Effect of short-term annealing on the microstructures and flow properties of an Al–1% Mg alloy processed by high-pressure torsion, Mater. Sci. Eng. A 615 (2014) 231-239.

[19] T.A. Lebedkina, M.A. Lebyodkin, T.T. Lamark, M. Janeček, Y. Estrin, Effect of equal channel angular pressing on the Portevin–Le Chatelier effect in an Al3Mg alloy, Mater. Sci. Eng. A 615 (2014) 7-13.

[20] H.-J. Lee, J.-K. Han, S. Janakiraman, B. Ahn, M. Kawasaki, T.G. Langdon, Significance of grain refinement on microstructure and mechanical properties of an Al-3% Mg alloy processed by high-pressure torsion, J. Alloys Compd.. 686 (2016) 998-1007.

[21] J. Wang, Y. Iwahashi, Z. Horita, M. Furukawa, M. Nemoto, R.Z. Valiev, T.G. Langdon, An investigation of microstructural stability in an Al-Mg alloy with submicrometer grain size, Acta Mater. 44 (1996) 2973-2982.

[22] D.G. Morris, M.A. Muñoz-Morris, Microstructure of severely deformed Al-3Mg and its evolution during annealing, Acta Mater. 50 (2002) 4047-4060.

[23] P.B. Prangnell, J.S. Hayes, J.R. Bowen, P.J. Apps, P.S. Bate, Continuous recrystallisation of lamellar deformation structures produced by severe deformation, Acta Mater. 52 (2004) 3193-3206.

[24] K. Dám, P. Lejček, A. Michalcová, In situ TEM investigation of microstructural behavior of superplastic Al–Mg–Sc alloy, Mater. Charact. 76 (2013) 69-75.

[25] S. Lee, A. Utsunomiya, H. Akamatsu, K. Neishi, M. Furukawa, Z. Horita, T.G. Langdon, Influence of scandium and zirconium on grain stability and superplastic ductilities in ultrafine-grained Al–Mg alloys, Acta Mater. 50 (2002) 553-564.

[26] M.J. Jones, F.J. Humphreys, Interaction of recrystallization and precipitation: The effect of Al_3Sc on the recrystallization behaviour of deformed aluminium, Acta Mater. 51 (2003) 2149-2159.

[27] M. Ferry, N.E. Hamilton, F.J. Humphreys, Continuous and discontinuous grain coarsening in a fine-grained particle-containing Al–Sc alloy, Acta Mater. 53 (2005) 1097-1109.

[28] D. Yuzbekova, A. Mogucheva, R. Kaibyshev, Superplasticity of ultrafine-grained Al–Mg–Sc–Zr alloy, Mater. Sci. Eng. A 675 (2016) 228-242.

[29] S. Malopheyev, S. Mironov, I. Vysotskiy, R. Kaibyshev, Superplasticity of friction-stir welded Al–Mg–Sc sheets with ultrafine-grained microstructure, Mater. Sci. Eng. A 649 (2016) 85-92.

[30] Yu.A. Filatov, V.I. Yelagin, V.V. Zakharov, New Al-Mg-Sc alloys, Mater. Sci. Eng. A 280 (2000) 97-101.

[31] J. Røyset, N. Ryum, Scandium in aluminium alloys, Int. Mater. Rev. 50 (2005) 19-44.

[32] Z. Horita, M. Furukawa, M. Nemoto, A.J. Barnes, T.G. Langdon, Superplastic forming at high strain rates after severe plastic deformation, Acta Mater. 48 (2000) 3633-3640.

[33] S. Komura, Z. Horita, M. Furukawa, M. Nemoto, T.G. Langdon, An evaluation of the flow behavior during high strain rate superplasticity in an Al-Mg-Sc Alloy, Metall. Mater. Trans. A 32 (2001) 707-716.

[34] S. Komura, M. Furukawa, Z. Horita, M. Nemoto, T.G. Langdon, Optimizing the procedure of equal-channel angular pressing for maximum superplasticity, Mater. Sci. Eng. A 297 (2001) 111-118.

[35] F. Musin, R. Kaibyshev, Y. Motohashi, G. Itoh, High strain rate superplasticity in a commercial Al–Mg–Sc alloy, Scripta Mater. 50 (2004) 511-516.

[36] E. Avtokratova, O. Sitdikov, M. Markushev, R. Mulyukov, Extraordinary high-strain rate superplasticity of severely deformed Al–Mg–Sc–Zr alloy, Mater. Sci. Eng. A 538 (2012) 386-390.

[37] E. Avtokratova, O. Sitdikov, O. Mukhametdinova, M. Markushev, S.V.S. Narayana Murty, M.J.N.V. Prasad, B.P. Kashyap, Microstructural evolution in Al–Mg–Sc–Zr

alloy during severe plastic deformation and annealing, J. Alloys Compd.. 673 (2016) 182-194.

[38] G. Sakai, Z. Horita, T.G. Langdon, Grain refinement and superplasticity in an aluminum alloy processed by high-pressure torsion, Mater. Sci. Eng. A 393 (2005) 344-351.

[39] Z. Horita, T.G. Langdon, Achieving exceptional superplasticity in a bulk aluminum alloy processed by high-pressure torsion, Scripta Mater. 58 (2008) 1029-1032.

[40] Y. Harai, K. Edalati, Z. Horita, T.G. Langdon, Using ring samples to evaluate the processing characteristics in high-pressure torsion, Acta Mater. 57 (2009) 1147-1153.

[41] P.H.R. Pereira, Y. Huang, T.G. Langdon, Examining the mechanical properties and superplastic behaviour in an Al-Mg-Sc alloy after processing by HPT, Lett. Mater. 5 (2015) 294-300.

[42] R.Z. Valiev, N.A. Enikeev, M.Yu. Murashkin, V.U. Kazykhanov, X. Sauvage, On the origin of the extremely high strength of ultrafine-grained Al alloys produced by severe plastic deformation, Scripta Mater. 63 (2010) 949-952.

[43] N. Kumar, R.S. Mishra, Additivity of strengthening mechanisms in ultrafine grained Al–Mg–Sc alloy, Mater. Sci. Eng. A 580 (2013) 175-183.

[44] D. Zhemchuzhnikova, R. Kaibyshev, Mechanical behavior of an Al–Mg–Mn–Sc alloy with an ultrafine grain structure at cryogenic temperatures, Adv. Eng. Mater. 17(12) (2015) 1804-1811.

[45] A. Mogucheva, D. Yuzbekova, R. Kaibyshev, T. Lebedkina, M. Lebyodkin, Effect of grain refinement on jerky flow in an Al-Mg-Sc Alloy, Metall. Mater. Trans. A 47 (2016) 2093-2106.

[46] Y. Ye, P. Li, L.S. Novikov, V.S. Avilkina, L. He, Comparison of residual microstructures associated with impact craters in Al−Sc and Al−Ti alloys, Acta Mater. 58 (2010) 2520-2526.

[47] W.G. Zhang, Y.C. Ye, L.J. He, P.J. Li, X. Feng, L.S. Novikov, Dynamic response and microstructure control of Al–Sc binary alloy under high-speed impact, Mater. Sci. Eng. A 578 (2013) 35-45.

[48] U. Andrade, M.A. Meyers, K.S. Vecchio, A.H. Chokshi, Dynamic recrystallization in high-strain, high-strain-rate plastic deformation of copper, Acta Mater. 42 (1994) 3183-3195.

[49] J.A. Hines, K.S. Vecchio, Recrystallization kinetics within adiabatic shear bands, Acta Mater. 45 (1997) 635-649.

[50] L. Zhen, G.A. Li, J.S. Zhou, D.Z. Yang, Micro-damage behaviors of Al–6Mg alloy impacted by projectiles with velocities of 1–3.2 km/s, Mater. Sci. Eng. A 391 (2005) 354-366.

[51] R. Kapoor, J.B. Singh, J.K. Chakravartty, High strain rate behavior of ultrafine-grained Al–1.5 Mg, Mater. Sci. Eng. A 496 (2008) 308-315.

[52] B. Mishra, C. Mondal, R. Goyal, P. Ghosal, K. Siva Kumar, V. Madhu, Plastic flow behavior of 7017 and 7055 aluminum alloys under different high strain rate test methods, Mater. Sci. Eng. A 612 (2014) 343-353.

[53] L. Wang, Y. Wang, A.P. Zhilyaev, A.V. Korznikov, S. Li, E. Korznikova, T.G. Langdon, Dynamic compressive behavior of ultrafine-grained pure Ti at elevated temperatures after processing by ECAP, J. Mater. Sci. 49 (2014) 6640-6647.

[54] L. Wang, Y.C. Wang, A.P. Zhilyaev, A.V. Korznikov, S.K. Li, E. Korznikova, T.G. Langdon, Microstructure and texture evolution in ultrafine-grained pure Ti processed by equal-channel angular pressing with subsequent dynamic compression, Scripta Mater. 77 (2014) 33-36.

[55] J.C. Yu, Z. Liu, Y. Dong, Z. Wang, Dynamic compressive property and failure behavior of extruded Mg-Gd-Y alloy under high temperatures and high strain rates, J. Magnesium Alloys 3 (2015) 134-141.

[56] S. Zhang, Y.C. Wang, A.P. Zhilyaev, D.V. Gunderov, S. Li, G.I. Raab, E. Korznikova, T.G. Langdon, Effect of temperature on microstructural stabilization and mechanical properties in the dynamic testing of nanocrystalline pure Ti, Mater. Sci. Eng. A 634 (2015) 64-70.

[57] S. Zhang, Y.C. Wang, A.P. Zhilyaev, E. Korznikova, S. Li, G.I. Raab, T.G. Langdon, Effect of grain size on compressive behaviour of titanium at different strain rates, Mater. Sci. Eng. A 656 (2015) 311-317.

[58] S. Zhang, Y.C. Wang, A.P. Zhilyaev, E. Korznikova, S. Li, G.I. Raab, T.G. Langdon, Temperature and strain rate dependence of microstructural evolution and dynamic mechanical behavior in nanocrystalline Ti, Mater. Sci. Eng. A 641 (2015) 29-36.

[59] M. Furukawa, Y. Iwahashi, Z. Horita, M. Nemoto, T.G. Langdon, The shearing characteristics associated with equal-channel angular pressing, Mater. Sci. Eng. A 257 (1998) 328-332.

[60] Y. Iwahashi, J. Wang, Z. Horita, M. Nemoto, T.G. Langdon, Principle of equal-channel angular pressing for the processing of ultra-fine grained materials, Scripta Mater. 35 (1996) 143-146.

[61] G.T. Gray, Classic split-Hopkinson pressure bar testing, in: ASM Metals Handbook: Mechanical Testing and Evaluation, vol. 8, ASM International, Metals Park (OH), 2000: 462.

[62] W.F. Hosford, R.M. Caddell, Metal Forming: Mechanics and Metallurgy, third ed., Cambridge University Press, New York, 2007.

[63] ASM Metals Handbook: Properties and Selection on Nonferrous Alloys and Special-Purpose Materials, vol. 2, ASM International, Metals Park (OH), 1990.

[64] G.J. Fan, G.Y. Wang, H. Choo, P.K. Liaw, Y.S. Park, B.Q. Han, E.J. Lavernia, Deformation behaviour of an ultrafine-grained Al-Mg alloy at different strain rates, Scr. Mater. 52 (2005) 929-933.

[65] L. Ziani, S. Boudrahem, H. Ait-Amokhtar, M. Mehenni, B. Kedjar, Unstable plastic flow in Al-2%Mg alloy, effect of annealing process, Mater. Sci. Eng. A536 (2012) 239-243.

[66] D.A. Zhemchuzhnikova, M.A. Lebyodkin, T.A. Lebedkina, R.O. Kaibyshev, Unusual behavior of the Portevin-Le Chatelier effect in an AlMg alloy containing precipitates, Mater. Sci. Eng. A 639 (2015) 37-41.

[67] H. Ishikawa, F.A. Mohamed, T.G. Langdon, The influence of strain rate on ductility in the superplastic Zn-22% Al eutectoid, Phil Mag 32 (1975) 1269-1271.

[68] L.E. Murr, E.V. Esquivel, Observations of common microstructural issues associated with dynamic deformation phenomena: Twins, microbands, grain size effects, shear bands, and dynamic recrystallization, J. Mater. Sci. 39 (2004) 1153-1168.

[69] H. Hu, Texture of Metals, Texture 1 (1974) 233-258.

[70] C.A. Bronkhorst, S.R. Kalidindi, L. Anand, Polycrystalline plasticity and the evolution of crystallographic texture in FCC Metals, Phil. Trans. R. Soc. Lond. A 341 (1992) 443-477.

[71] M. Kawasaki, T.G. Langdon, Principles of superplasticity in ultrafine-grained materials, J. Mater. Sci. 42 (2007) 1782-1796.

[72] L.S. Tóth, B. Beausir, C.F. Gu, Y. Estrin, N. Scheerbaum, C.H.J. Davies, Effect of grain refinement by severe plastic deformation on the next-neighbor misorientation distribution, Acta Mater. 58 (2010) 6706-6716.

[73] J.K. Mackenzie, Second paper on statistics associated with the random disorientation of cubes, Biometrika 45 (1958) 229-240.

[74] S. Li, I.J. Beyerlein, M.A.M. Bourke, Texture formation during equal channel angular extrusion of fcc and bcc materials: comparison with simple shear, Mater. Sci. Eng. A 394 (2005) 66-77.

[75] I.J. Beyerlein, L.S. Tóth, Texture evolution in equal-channel angular extrusion, Prog. Mater. Sci. 54 (2009) 427-510.

[76] C.F. Gu, L.S. Tóth, C.H.J. Davies, Effect of strain reversal on texture and grain refinement in route C equal channel angular pressed copper, Scripta Mater. 65 (2011) 167-170.

[77] C.F. Gu, L.S. Tóth, The origin of strain reversal texture in equal channel angular pressing, Acta Mater. 59 (2011) 5749-5757.

[78] K. Furuno, H. Akamatsu, K. Oh-ishi, M. Furukawa, Z. Horita, T.G. Langdon, Microstructural development in equal-channel angular pressing using a 60º die, Acta Mater. 52 (2004) 2497-2507.

[79] E.A. Marquis, D.N. Seidman, D.C. Dunand, Effect of Mg addition on the creep and yield behavior of an Al–Sc alloy, Acta Mater. 51 (2003) 4751-4760.

[80] H. Hasegawa, S. Komura, A. Utsunomiya, Z. Horita, M. Furukawa, M. Nemoto, T.G. Langdon, Thermal stability of ultrafine-grained aluminum in the presence of Mg and Zr additions, Mater. Sci. Eng. A 265 (1999) 188-196.

[81] A.H. Chokshi, A. Rosen, J. Karch, H. Gleiter, On the validity of the Hall-Petch relationship in nanocrystalline materials, Scripta Mater. 23 (1989) 1679-1683.

[82] K.S. Kumar, H.V. Swygenhoven, S. Suresh, Mechanical behavior of nanocrystalline metals and alloys, Acta Mater. 51 (2003) 5743-5774.

[83] M.A. Meyers, A. Mishra, D.J. Benson, Mechanical properties of nanocrystalline materials, Prog. Mater. Sci. 51 (2006) 427-556.

[84] J.R. Trelewicz, C.A. Schuh, The Hall–Petch breakdown at high strain rates: Optimizing nanocrystalline grain size for impact applications, Appl. Phys. Lett. 93 (2008) 171916.

[85] E.N. Hahn, M.A. Meyers, Grain-size dependent mechanical behavior of nanocrystalline metals, Mater. Sci. Eng. A 646 (2015) 101-134.

[86] Z. Horita, T. Fujinami, M. Nemoto, T.G. Langdon, Equal-channel angular pressing of commercial aluminum alloys: Grain refinement, thermal stability and tensile properties, Metall. Mater. Trans. A 31 (2000) 691-701.

[87] N. Tsuji, in: Y.T. Zhu, V. Varyukhin (Eds.), Nanostructured Materials by High-pressure Severe Plastic Deformation, Springer Netherlands, 2006, 227.

[88] C. Kwan, Z. Wang, S.B. Kang, Mechanical behavior and microstructural evolution upon annealing of the accumulative roll-bonding (ARB) processed Al alloy 1100, Mater. Sci. Eng. A 480 (2008) 148-159.

[89] A. Azimi, S. Tutunchilar, G. Faraji, M.K. Besharati Givi, Mechanical properties and microstructural evolution during multi-pass ECAR of Al 1100–O alloy, Mater. Des. 42 (2012) 388-394.

[90] M. Furukawa, Z. Horita, M. Nemoto, R.Z. Valiev, T.G. Langdon, Microhardness measurements and the Hall-Petch relationship in an Al-Mg alloy with submicrometer grain size, Acta Mater. 44 (1996) 4619-4629.

[91] M. Furukawa, Z. Horita, M. Nemoto, R.Z. Valiev, T.G. Langdon, Factors influencing the flow and hardness of materials with ultrafine grain sizes, Philos. Mag. A. 78 (1998) 203-216.

[92] J.S. Hayes, R. Keyte, P.B. Prangnell, Effect of grain size on tensile behaviour of a submicron grained Al-3 wt-%Mg alloy produced by severe deformation, Mater. Sci. Technol. 16 (2000) 1259-1263.

[93] N. Kumar, R.S. Mishra, C.S. Huskamp, K.K. Sankaran, Critical grain size for change in deformation behavior in ultrafine grained Al–Mg–Sc alloy, Scripta Mater. 64 (2011) 576-579.

[94] P. Bazarnik, Y. Huang, M. Lewandowska, T.G. Langdon, Structural impact on the Hall-Petch relationship in an Al-5Mg alloy processed by high-pressure torsion, Mater. Sci. Eng. A 626 (2015) 9-15.

[95] G. Sha, L. Yao, X. Liao, S.P. Ringer, Z.C. Duan, T.G. Langdon, Segregation of solute elements at grain boundaries in an ultrafine grained Al–Zn–Mg–Cu alloy, Ultramicroscopy 111 (2011) 500-505.

[96] X. Sauvage, G. Wilde, S.V. Divinski, Z. Horita, R.Z. Valiev, Grain boundaries in ultrafine grained materials processed by severe plastic deformation and related phenomena, Mater. Sci. Eng. A 540 (2012) 1-12.

[97] X. Sauvage, A. Ganeev, Y. Ivanisenko, N. Enikeev, M. Murashkin, R. Valiev, Grain boundary segregation in UFG alloys processed by severe plastic deformation, Adv. Eng. Mater. 14(11) (2012) 968-974.

[98] X. Sauvage, N. Enikeev, R. Valiev, Y. Nasedkina, M. Murashkin, Atomic-scale analysis of the segregation and precipitation mechanisms in a severely deformed Al–Mg alloy, Acta Mater. 72 (2014) 125-136.

[99] G.J. Tucker, M.A. Tschopp, D.L. McDowell, Evolution of structure and free volume in symmetric tilt grain boundaries during dislocation nucleation, Acta Mater. 58 (2010) 6464-6473.

[100] K. Kinoshita, T. Shimokawa, T. Kinari, Grain boundary structure dependence of extrinsic grain boundary dislocation emission phenomena: A molecular dynamics study, Mater. Trans. 53 (2012) 147-155.

[101] D. Farkas, Atomistic simulations of metallic microstructures, Curr. Opin. Solid State Mater. Sci. 17 (2013) 284-297.

[102] F. Abdeljawad, S.M. Foiles, Stabilization of nanocrystalline alloys via grain boundary segregation: A diffuse interface model, Acta Mater. 101 (2015) 159-171.

[103] L.E. Karkina, I.N. Karkin, A.R. Kuznetsov, I.K. Razumov, P.A. Korzhavyi, Yu.N. Gornostyrev, Solute–grain boundary interaction and segregation formation in Al: First principles calculations and molecular dynamics modelling, Comp. Mater. Sci. 112 (2016) 18-26.

[104] A. Van den Beukel, U.F. Kocks, The strain dependence of static and dynamic strain-aging, Acta Metall. 30 (1982) 1027-1034.

[105] W.A. Curtin, D.L. Olmsted, L.G. Hector, A predictive mechanism for dynamic strain ageing in aluminium-magnesium alloys, Nat. Mater. 5 (2006) 875-880.

[106] H. Aboulfadl, J. Deges, P. Choi, D. Raabe, Dynamic strain aging studied at the atomic scale, Acta Mater. 86 (2015) 34-42.

[107] P.R. Cetlin, A.Ş. Güleç, R.E. Reed-Hill, Serrated flow in aluminium 6061 alloy, Metall. Trans. 4 (1973) 513-517.

[108] A.M. Giarola, P.H.R. Pereira, P.A. Stemler, A.E.M. Pertence, H.B. Campos, M.T.P. Aguilar, P.R. Cetlin, Strain heterogeneities in the rolling direction of steel sheets submitted to the skin pass: A finite element analysis, J. Mater. Process. Technol. 216 (2015) 234-247.

[109] P. Yavari, T.G. Langdon, An examination of the breakdown in creep by viscous glide in solid solution alloys at high stress levels, Acta Metall. 30 (1982) 2181-2196.

[110] J.E. Bird, A.K. Mukherjee, J.E. Dorn, in :D.G. Brandon, A. Rosen (Eds.), Quantitative Relation between Properties and Microstructure, Israel Universities Press, Jerusalem, Israel (1969) 255-342.

[111] W.R. Cannon, T.G. Langdon, Review: Creep of ceramics: Part 2 An examination of flow mechanisms, J. Mater. Sci. 23 (1988) 1-20.

[112] F.A. Mohamed, T.G. Langdon, Deformation mechanism maps based on grain size, Metall. Trans. 5 (1974) 2339-2345.

Fig. 1. Schematic illustration of the samples used during (a) ECAP processing, (b) tensile testing and (c) dynamic testing.

Fig. 2. True stress vs true strain curves for samples of the solution treated Al-3Mg-0.2Sc alloy (broken lines) before and (solid lines) after processing by ECAP and further dynamic testing at 4.0×10^3 s^{-1} within the temperature range from 298 to 673 K.

Fig. 3. Variation of the true stress at a true strain of 0.05 with the strain rate for samples of the solution treated Al-3Mg-0.2Sc alloy (a) before and (b) after processing by ECAP and further mechanical testing within the temperature range from 298 to 673 K.

Fig. 4. OIM images for (a) the solution treated Al-3Mg-0.2Sc alloy and after dynamic testing at 4.0×10^3 s^{-1} at (b) 298 and (c) 673 K.

Fig. 5. Texture represented as {111} pole figures for (a) the solution treated Al-3Mg-0.2Sc alloy and after dynamic testing at 4.0 x 10^3 s^{-1} at (b) 298 and (c) 673 K.

Fig. 6. OIM images of the ECAP-processed Al-3Mg-0.2Sc alloy after (a) annealing at 673 K for 10 min, (b) tensile testing at 3.3×10^{-3} s^{-1} at 673 K and dynamic testing at 4.0×10^3 s^{-1} (c) at 298 and (d) at 673 K.

Fig. 7. Histograms of the misorientation angles for the ECAP-processed Al-3Mg-0.2Sc alloy after (a) annealing at 673 K for 10 min, (b) tensile testing at 3.3×10^{-3} s^{-1} at 673 K and dynamic testing at 4.0×10^3 s^{-1} (c) at 298 and (d) at 673 K.

Fig. 8. Texture represented as {111} pole figures for the ECAP-processed Al-Mg-Sc alloy after (a) annealing at 673 K for 10 min, (b) tensile testing at 3.3×10^{-3} s^{-1} at 673 K and dynamic testing at 4.0×10^3 s^{-1} (c) at 298 and (d) at 673 K.

Fig. 9. The Hall-Petch relationship in commercially pure aluminium [86-89], Al-Mg alloys [10,18,20,51,90-92] and Al-Mg-Sc alloys [37,42-44,93].

Fig. 10. Average grain boundary spacing, $\overline{L}$, vs. modulus-compensated stress, σ/G, for the Al-1.5Mg alloy [51] and the Al-3Mg-0.2Sc alloy processed by ECAP and then mechanically tested at various temperatures and strain rates: the two broken lines denote the measured grain sizes in the Al-Mg-Sc alloy immediately after ECAP ($\overline{L}_{(0,298\ K)}$) and after ECAP and annealing at 673 K for 10 min ($\overline{L}_{(0,673\ K)}$) and the solid line represents the theoretical prediction for λ using Eq. (3).

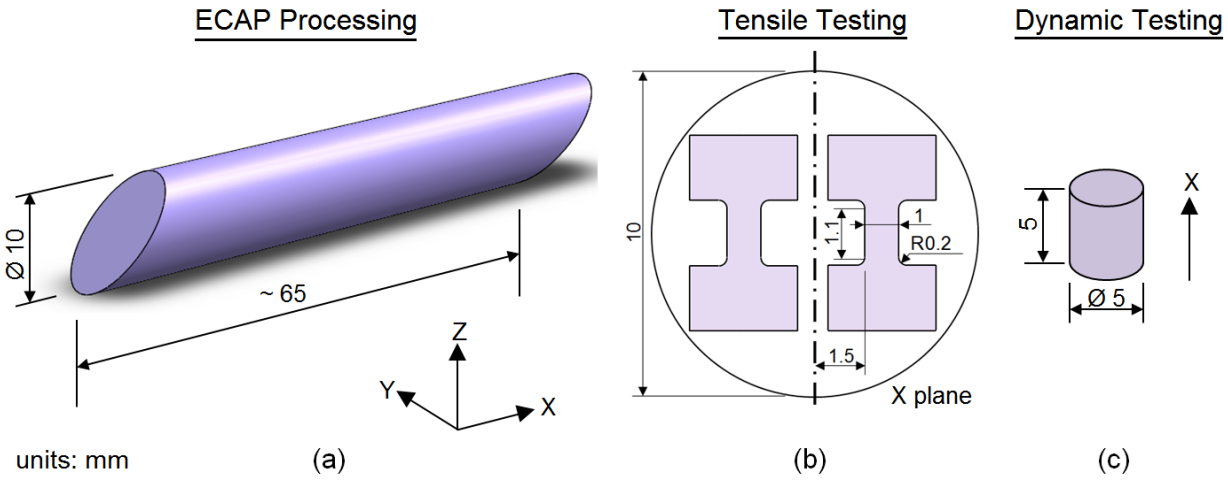

Fig. 1

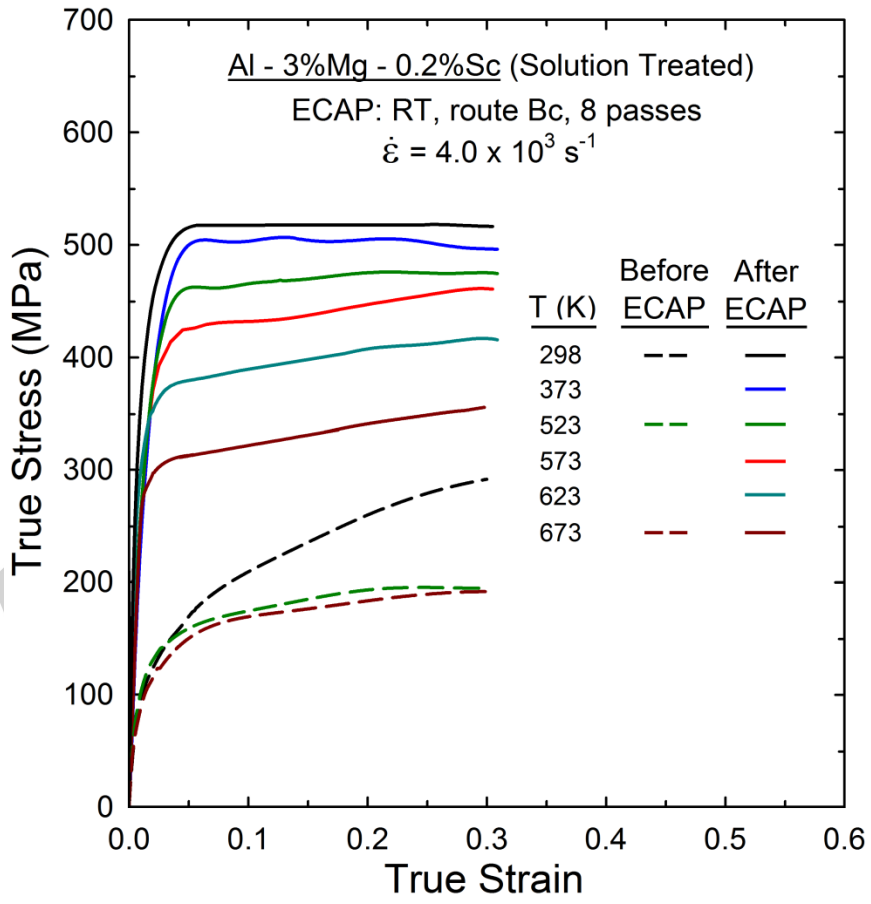

Fig. 2

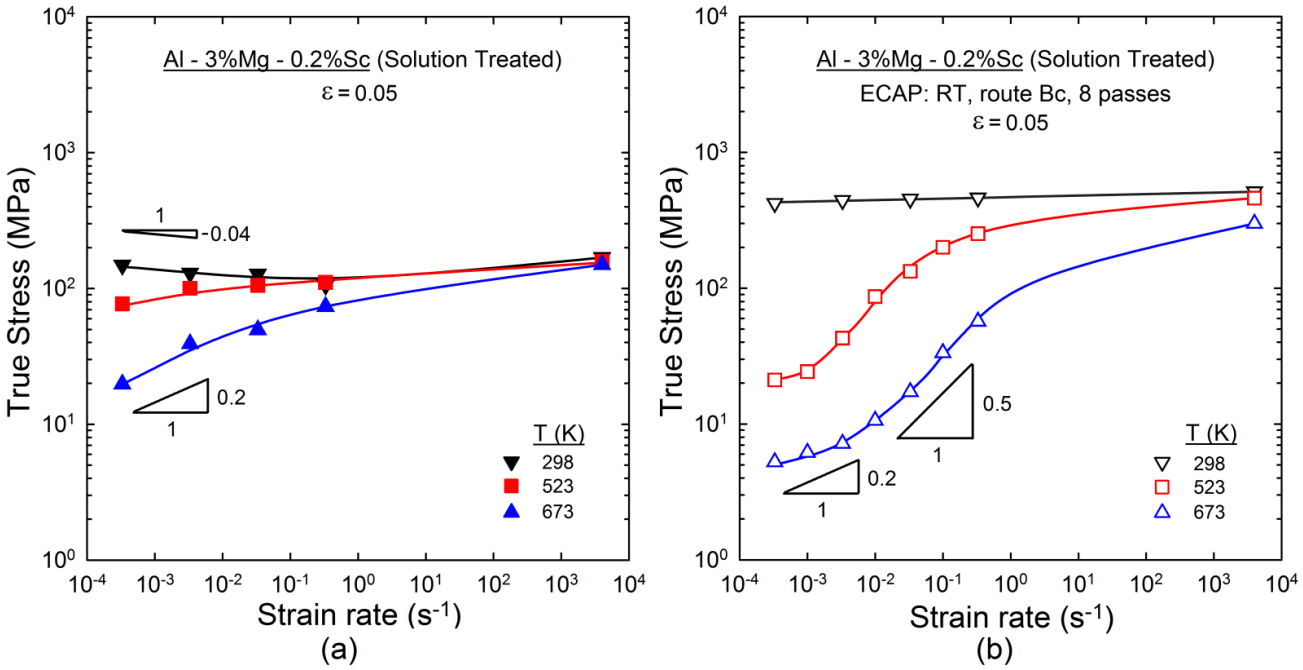

Fig. 3

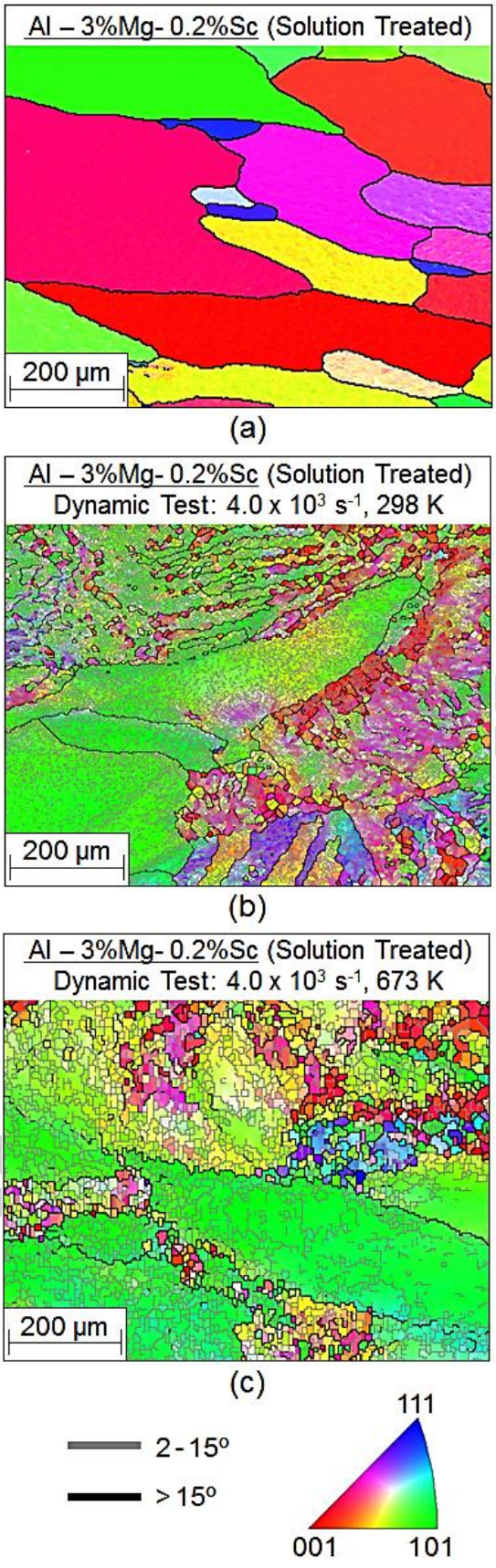
Al – 3%Mg- 0.2%Sc (Solution Treated)
200 µm
(a)
Al – 3%Mg- 0.2%Sc (Solution Treated)
Dynamic Test: 4.0 x 10³ s⁻¹, 298 K
200 µm
(b)
Al – 3%Mg- 0.2%Sc (Solution Treated)
Dynamic Test: 4.0 x 10³ s⁻¹, 673 K
200 µm
(c)
2 - 15º
> 15º
111
001
101

Fig. 4

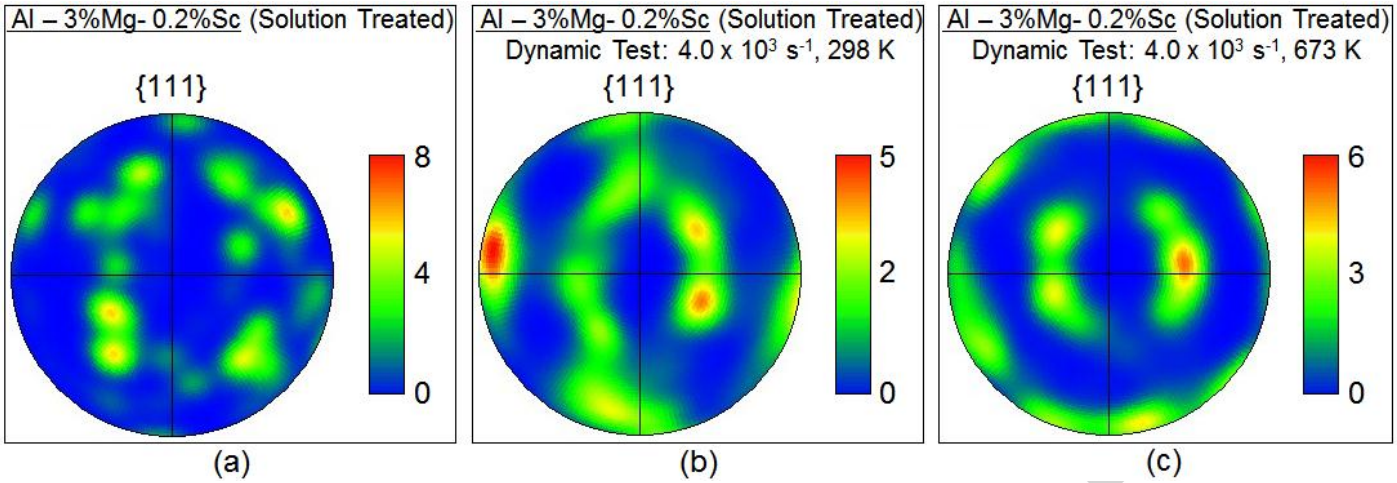

Fig. 5

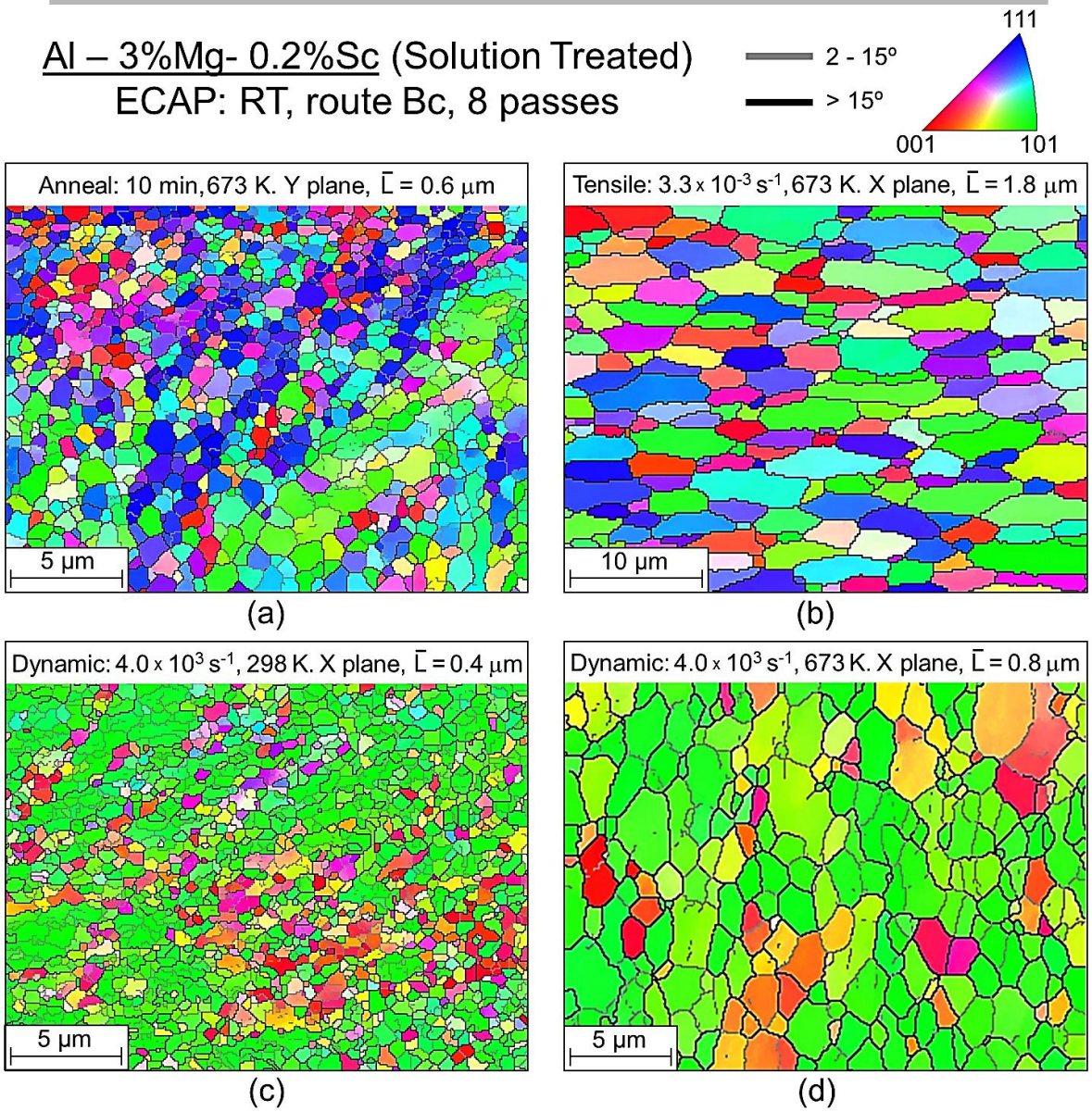

Fig. 6

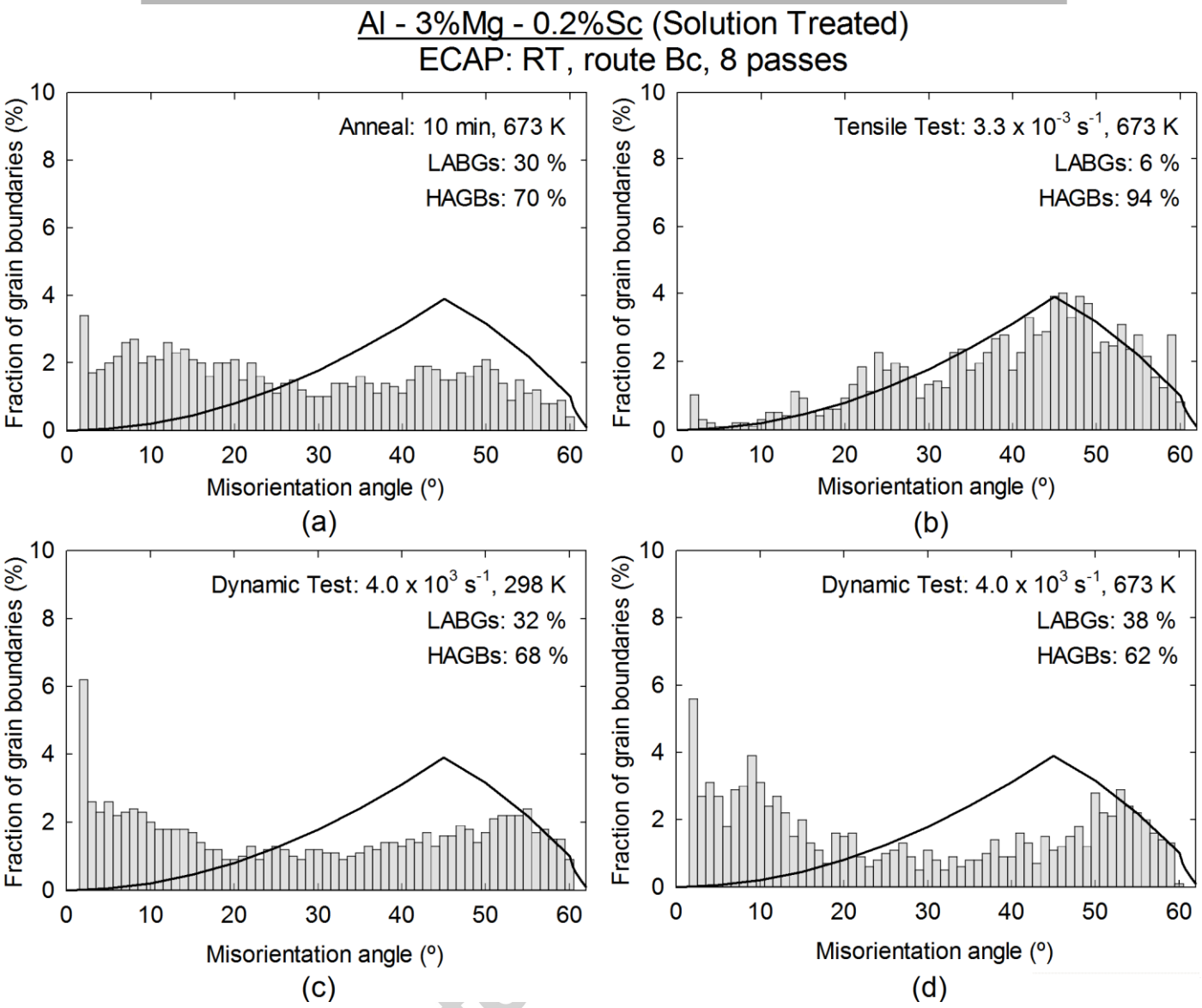

Fig. 7

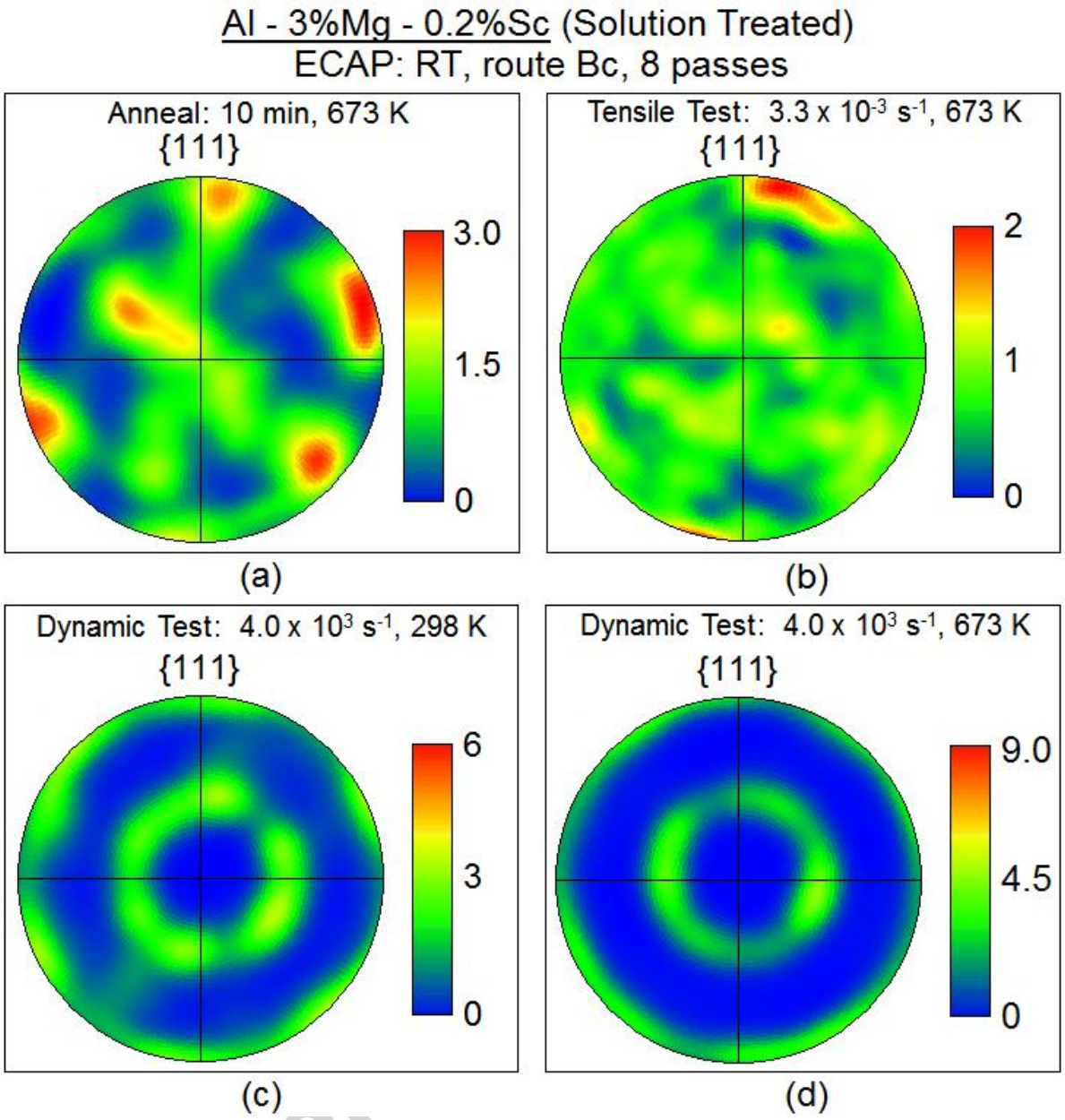
Al - 3%Mg - 0.2%Sc (Solution Treated)
ECAP: RT, route Bc, 8 passes
Anneal: 10 min, 673 K
{111}
3.0
1.5
0
(a)
Tensile Test: 3.3 x 10-3 s-1, 673 K
{111}
2
1
0
(b)
Dynamic Test: 4.0 x 10³ s-1, 298 K
{111}
6
3
0
(c)
Dynamic Test: 4.0 x 10³ s-1, 673 K
{111}
9.0
4.5
0
(d)

Fig. 8

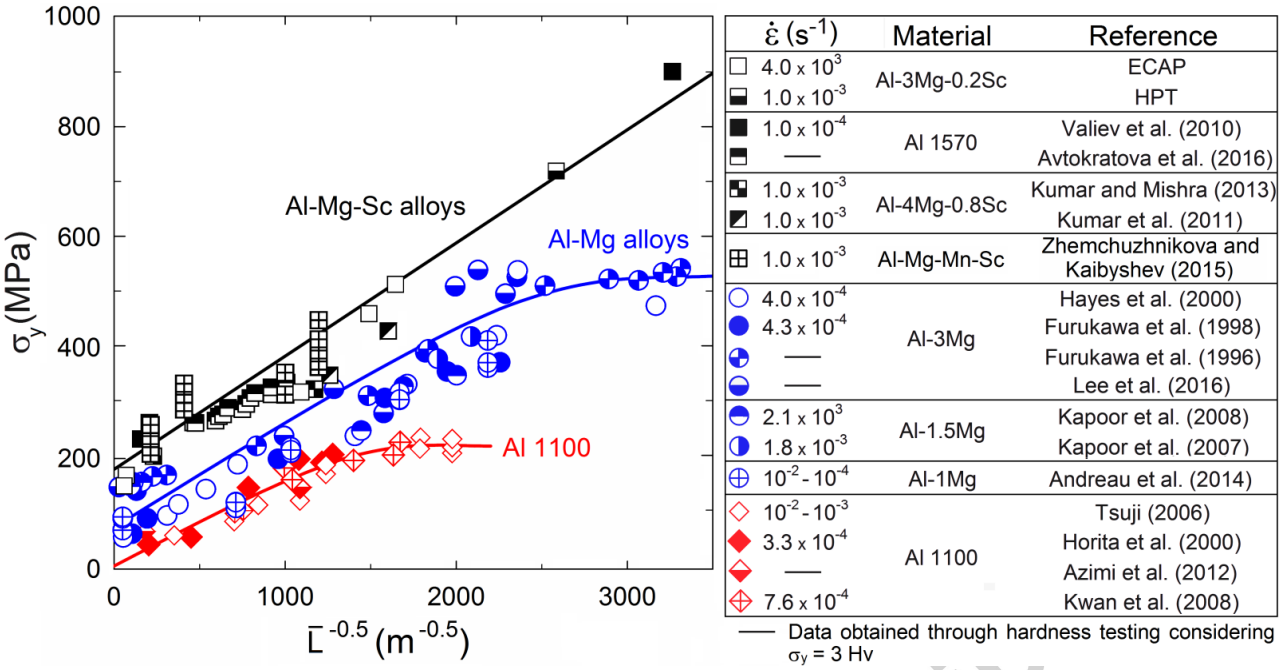

Fig. 9

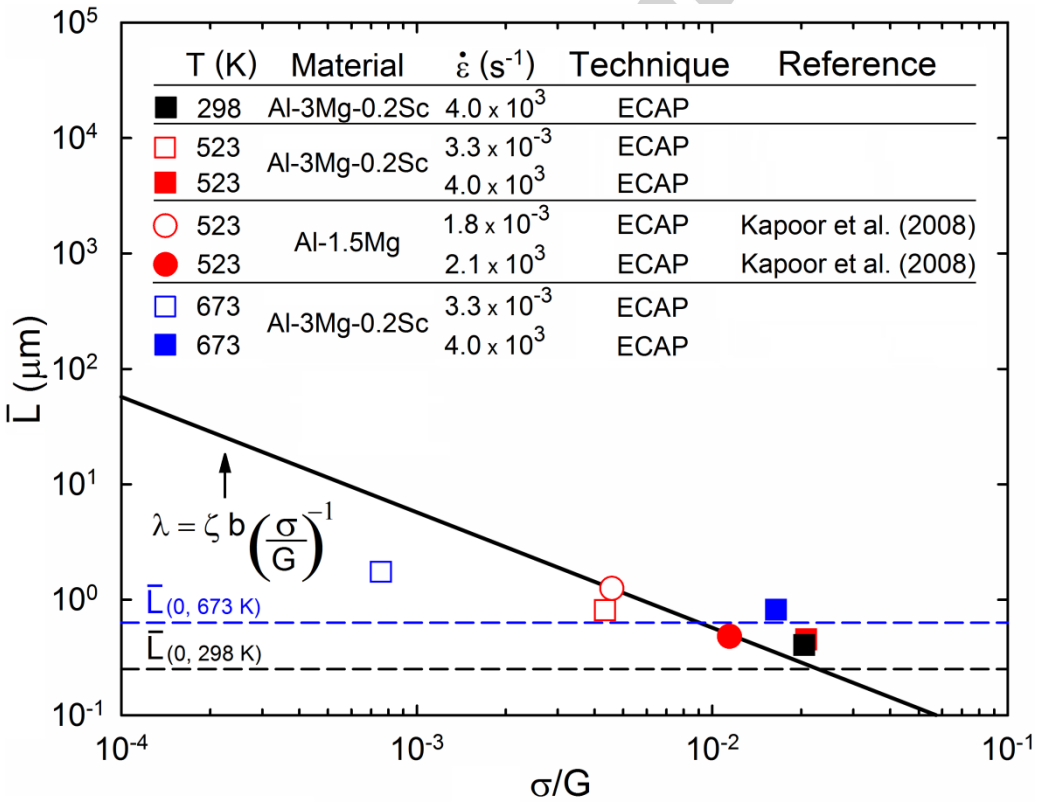

Fig. 10